Supporting Information

Yurchenko et al. 10.1073/pnas.1324219111

The experimental data on methane transition intensities are far from complete, especially at the elevated temperatures. As an illustration, Fig. S1 shows the $T = 1{,}500$ K absorption spectra of methane generated using the high-resolution transmission molecular absorption (HITRAN) 2012 database. To be able to use HITRAN for simulating spectra for temperatures different from 296 K, the information on the energy of the lower state as well as on its degeneracy is required. Only 250,000 lines of $^{12}CH_4$ out of 336,830 lines from HITRAN 2012 contain this information. Only these intensities are shown in Fig. S1. The 10to10 spectrum of methane is shown as a background plotted using all 9,819,605,160 lines. The line list covers the frequency range up to 12,000 cm^{-1}.

Density of Lines

Fig. S2, *Upper*, shows the density of lines per cm^{-1} of the absorption spectra of CH_4 computed with 10to10 at $T = 1{,}500$ K, where only the transitions stronger than 10^{-29} cm/molecule are accounted for. The highest density of lines appears to be in the 7,300-cm^{-1} (1.37-μm) region. The highest maxima coincide with the centers of the strongest bands; see Fig. S2, *Lower*, where an overview of the absorption spectra at $T = 1{,}500$ K is given.

Potential Energy and Dipole Moment Surfaces

The necessary prerequisites for computing a molecular spectrum and a line list are an appropriate potential energy surface (PES) and dipole moment surfaces (DMSs). The rovibrational energies and wave functions were computed using a spectroscopic PES obtained through a least-squares fit to the $^{12}CH_4$ experimental energy levels derived from the frequencies collected in the HITRAN 2008 database (1). In these fittings, only the energy values below $hc \cdot 6{,}100$ cm^{-1} and with $J \leq 4$ were used. The quality of the empirical PES can be assessed by the accuracy of the fit. The fitting root-mean-square error is $hc \cdot 0.1$ cm^{-1} for all 317 energy levels included. In our fitting procedure the wave functions obtained by solving the Schrödinger equation for the original PES serve as basis functions (2). The refined potential energy function represented by a sixth-order expansion will be reported elsewhere (3). To evaluate the Einstein coefficients, the previously computed (4) ab initio, CH_4 DMSs were used. These DMSs were generated at 114,000 distinct geometries using the coupled cluster theory at the high, CCSD(T)-F12c/aug-ccpVTZ-F12 level. The DMSs are represented by an analytic fit to these computed points based on sixth-order symmetry-adapted expansions in terms of the nine internal coordinates. These DMSs have been shown to accurately describe the experimental band intensities when these are available; see Table S1 and ref. 4 for a more detailed analysis.

To reach higher accuracy for the line positions currently inaccessible by the ab initio methods, the PES was adjusted through least-squares fitting to the experimental rovibrational energies. Most of the energies known experimentally are reproduced with our PES within 0.4 cm^{-1}. As an additional step in the improvement of the calculation accuracy, the theoretical band centers were substituted by the empirical ones, where available. This approach allows us to propagate the accuracy of the pure rotational spectrum (root-mean-square error of 0.01 cm^{-1} for all pure-rotational lines with $J \leq 18$) to the rovibrational line positions within vibrationally excited bands. The resulted accuracy of the line positions is illustrated in Fig. 1 in case of the ν_3 fundamental band and can be also seen in Fig. 4 of the T 4.5 dwarf spectrum in region of 1.6 and 2.2 μm (see also ref. 3 for more detailed comparisons). The accuracy of the line positions deteriorates at high vibrational excitations, up to 10–40 cm^{-1} and more above $hc \cdot 8{,}000$ cm^{-1}, which is one of the reasons for the upper frequency limit of 12,000 cm^{-1} (3). To extend it to even higher frequencies and thus to approach the relatively weak methane band at 0.89 μm (5, 6), a better quality PES will be required.

Modeling the Spectra of Exoplanets

We used a line-by-line integration scheme to model transmission of the radiation from the parent star through the atmosphere of the orbiting planet as a function of wavelength in the primary transit geometry. A transit depth is represented by the ratio of the radii of the planet and the star. The compositions are estimated by comparing to any available observations. The details of the model can be found in refs. 7 and 8. Fig. S3 shows the transmission spectra of the atmosphere of HD 189733b generated using theoretical (10to10) and experimental (HITRAN) line lists of CH_4 using three different models. The model corresponding to the larger contribution of CH_4 (mixing ratio of 5×10^{-4}) exhibits a more pronounced effect from the new CH_4 data.

Fig. S4 shows the transmission spectra of the atmosphere of GJ 436b from a slightly different perspective than Fig. 5: (*i*) the linear scale is used here to show the long wavelengths in more detail and (*ii*) the lower display presents the difference between the ratios R_p/R_* obtained for 10to10 and HITRAN. The observational data are from refs. 9 and 10.

1. Rothman LS, et al. (2009) *J Quant Spectrosc Radiat Transf* 110(9-10):533–572.
2. Yurchenko SN, Barber RJ, Tennyson J, Thiel W, Jensen P (2011) Towards efficient refinement of molecular potential energy surfaces: Ammonia as a case study. *J Mol Spectrosc* 268(1-2):123–129.
3. Yurchenko SN, Tennyson J (2014) Exomol line lists IV: The rotation-vibration spectrum of methane up to 1500 K. *Mon Not R Astron Soc* 440(2):1649–1661.
4. Yurchenko SN, Tennyson J, Barber RJ, Thiel W (2013) Vibrational transition moments of CH_4 from the first principles. *J Mol Spectrosc* 291:69–76.
5. Oppenheimer BR, Kulkarni SR, Matthews K, van Kerkwijk MH (1998) The spectrum of the brown dwarf Gliese 229B. *Astrophys J* 502(2):932–943.
6. Burgasser AJ, Kirkpatrick JD, Liebert J, Burrows A (2003) The spectra of T dwarfs. II. Red optical data. *Astrophys J* 594(1):510–524.
7. Tinetti G, Tennyson J, Griffith CA, Waldmann I (2012) Water in exoplanets. *Philos Trans A Math Phys Eng Sci* 370(1968):2749–2764.
8. Hollis MDJ, Tessenyi M, Tinetti G (2013) TAU: A 1D radiative transfer code for transmission spectroscopy of extrasolar planet atmospheres. *Comput Phys Commun* 184(10):2351–2361.
9. Beaulieu JP, et al. (2011) Methane in the atmosphere of the transiting hot Neptune GJ436b? *Astrophys J* 731(1):16.
10. Knutson HA, et al. (2011) A Spitzer transmission spectrum for the exoplanet GJ 436b, evidence for stellar variability, and constraints on dayside flux variations. *Astrophys J* 735(1):27.

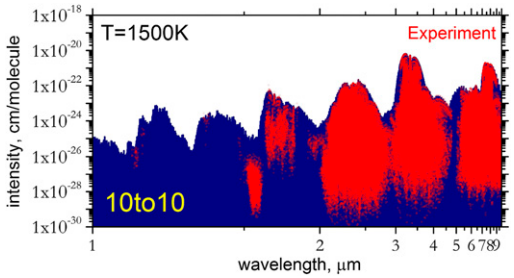

Fig. S1. Absorption intensities of methane at $T = 1{,}500$ K: Experimental (red circles) data set, from HITRAN 2012 (1), at this temperature contains less than 300,000 lines vs. the almost 10 billion synthetic lines from 10to10 (blue bars) shown as background. In the synthetic spectrum; only lines with maximal intensity at each 0.1 cm^{-1} wavenumber bin are shown.

1. Rothman LS, et al. (2013) The HITRAN 2012 molecular spectroscopic database. *J Quant Spectrosc Radiat Transf* 130:4–50.

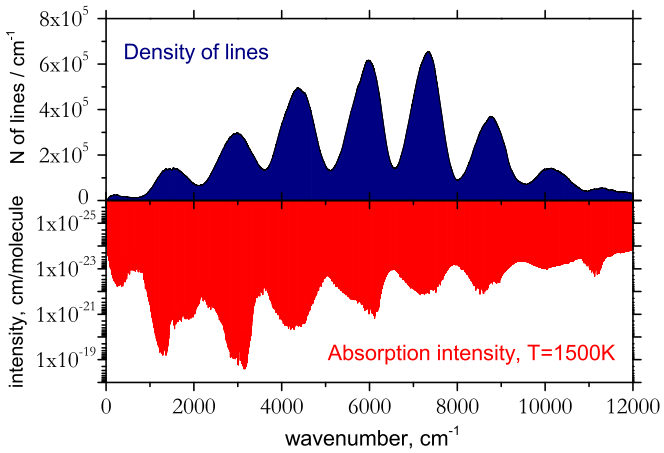

Fig. S2. The density of lines ($I \leq 10^{-29}$ cm/molecule) and an overview of the absorption spectra of CH_4 at $T = 1{,}500$ K obtained using the 10to10 line list.

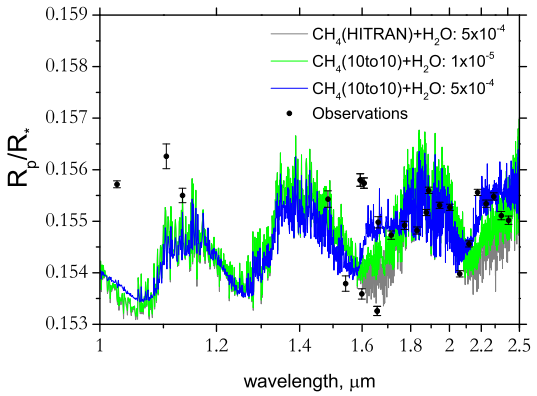

Fig. S3. $CH_4 + H_2O$ transmission spectra of the atmosphere of HD 189733b at 1,200 K obtained using TAU in conjunction with three models. Model 1: CH_4 (10to10) + H_2O, mixing ratio is 5×10^{-4} (both H_2O and CH_4); model 2: CH_4 (10to10) + H_2O, mixing ratio is 1×10^{-5} (both H_2O and CH_4); model 3: CH_4 (HITRAN) + H_2O, mixing ratio is 5×10^{-4} (both H_2O and CH_4). The offset is 4.5%.

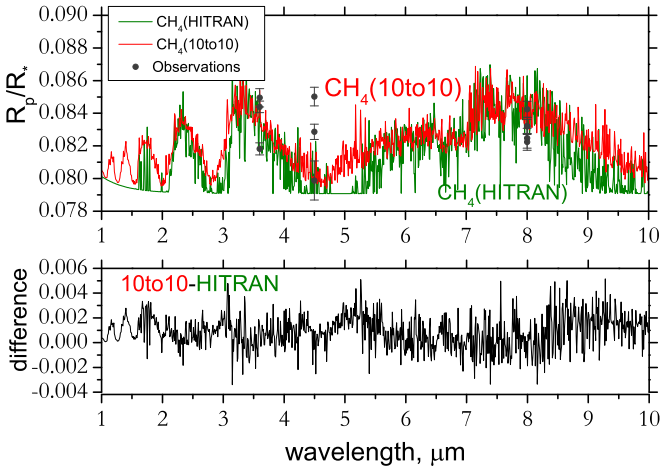

Fig. S4. (*Upper*) TAU transmission spectra of the atmosphere of GJ 436b at 700 K obtained using the 10to10 and HITRAN (methane) line lists. (*Lower*) The difference between these spectra (10to10 − HITRAN). The observational data points are from Beaulieu et al. (1) and Knutson et al. (2).

1. Beaulieu JP, et al. (2011) Methane in the atmosphere of the transiting hot Neptune GJ436b? *Astrophys J* 731(1):16.
2. Knutson HA, et al. (2011) A Spitzer transmission spectrum for the exoplanet GJ 436b, evidence for stellar variability, and constraints on dayside flux variations. *Astrophys J* 735(1):27.

Table S1. Experimental and theoretical integrated intensities (cm^{-2} atm^{-1}) for a number of selected bands of $^{14}CH_4$ at $T = 297$ K

Band	Band center, μm	Experiment	Theory
g.s.	66.67	0.00	0.00
N_4	7.63	127.68	125.20
$2\nu_4(A_1)$	3.87	0.02	0.02
$2\nu_4(F_2)$	3.83	1.05	0.88
$\nu_2 + \nu_4(F_2)$	3.53	6.63	5.83
$\nu_2 + \nu_4(F_1)$	3.53	2.51	1.86
$\nu_2 + \nu_4(F_1)$	3.51	2.51	1.86
ν_1	3.43	0.05	0.07
$\nu_3(F_2)$	3.31	269.92	281.13
$2\nu_2(A_1)$	3.26	0.09	0.13
$2\nu_2$(all)	3.26	0.70	0.59
$3\nu_4$(all)	2.56	0.83	0.84
$\nu_2 + 2\nu_4$(all)	2.42	0.92	0.76
$\nu_3 + \nu_4$(al)	2.31	10.24	11.15
$2\nu_2 + \nu_4$(a)	2.30	0.93	0.74
$3\nu_2$(all)	2.18	0.03000	0.02332

Experimental intensities are from ref. 1, and theoretical intensities are from this work. g.s., ground state.

1. Rothman LS, et al. (2013) The HITRAN 2012 molecular spectroscopic database. *J Quant Spectrosc Radiat Transf* 130:4–50.